scientific reports

Check for updates

OPEN

Study of the neutron radiation hardness of MAPD-3NK2 silicon photomultipliers

F. Ahmadov[1,2,3]✉, G. Ahmadov[2,4], A. Mammadli[1], A. Sadygov[1,2], Z. Sadygov[1,2], A. Jazbec[5], K. Ambrožič[5,8], M. Holik[6,7], R. Akbarov[1,2], S. Nuruyev[1], F. Mamadov[7], O. Okhrimenko[9], Yu. Shitov[7] & Yu. Yu. Bacherikov[9,10]✉

The radiation hardness of MAPD-3NK2 photodiodes with deep-buried pixel structures was evaluated under neutron irradiation at fluences ranging from 3.6×10^{9} to 3.6×10^{12} n_{eq}/cm^2. Irradiation induced dark current increase of up to 2060 times, a breakdown voltage shift of (0.37 ± 0.08) V, a photo signal amplitude reduction of (90.1 ± 0.4) %, and a tenfold degradation in amplitude resolution. Partial recovery was observed after 40 days of room-temperature annealing, with dark current decreasing by 35%.Similar performance changes were observed in photodiodes with artificially elevated dark current, indicating that excess current is the primary driver of degradation. This current likely impedes photoelectron detection by occupying pixels or failing to fully quench the avalanche process, thereby reducing photocurrent.

Silicon photomultipliers (SiPMs) are highly sensitive solid-state photon detectors that have gained widespread use in fields such as medical imaging[1], high-energy physics experiments[2], space instrumentation[3], and industrial applications. Compared to traditional photomultiplier tubes (PMTs), SiPMs offer advantages such as compact size, low operating voltage, high gain, and excellent single-photon detection capabilities[4–13]. However, in radiation-intensive settingssuch as space missions, nuclear reactors, and particle acceleratorsSiPMs face significant exposure to mixed radiation fluxes (e.g., gamma rays, electrons, protons, and neutrons), which can degrade their performance over time[14–24].

Neutron irradiation is a standard method for assessing the radiation hardness of materials and electronic devices due to its ability to cause bulk damage in semiconductors. This damage introduces defects that act as charge carrier traps and generation-recombination centers, resulting in increased dark current, shifts in breakdown voltage, and reduced photosensitivity, all of which impair SiPM performance[14–17]. Studies in space exploration (e.g., EIRSAT-1 and HERD) and high-energy physics (e.g., Ring Imaging Cherenkov detectors, Belle II, NA61@CERN, CBM@FAIR, BM@N, and NICA experiments) have identified neutron fluences of 1×10^{10} to 1×10^{13} n_{eq}/cm^2 as typical exposure levels over a detector's lifetime[18–27]. Given the increasing deployment of SiPMs in such environments, understanding their radiation tolerance and developing mitigation strategies are critical.

Extensive research exists on the radiation hardness of SiPMs with surface pixel structures[18–27]. For instance, Ref[18]. examined two SiPM types with 10 µm pixel pitches under neutron fluences up to 1.35×10^{12} n_{eq}/cm^2, observing dark current increases of 200–400 times with 3 mm aluminium shielding and up to 10 000 times without shielding, alongside evaluations of minimum ionizing particle signals and annealing behaviour. Ref[19]. tested FBK NUV-HD-RH UHD-DE SiPMs (15 µm pixel pitch) at fluences from 1×10^{9} n_{eq}/cm^2 to 1×10^{13} n_{eq}/cm^2, noting a dark current rise of up to 10 000 times, though breakdown voltage shifts were not reported; annealing effects were also studied.Ref[26]. investigated HPK SiPMs (10 µm cells, 10 000 pixels/mm^2), finding a 4 V breakdown voltage shift after proton irradiation to 10^{14} p/cm^2, but lacked detailed amplitude and dark

[1]Institute of Radiation Problems- Ministry of Science and Education, B.Vahabzade str.9, AZ1143 Baku, Azerbaijan. [2]Department of Nuclear Research of IDDA, Baku Shamakhy HW 20 km, Gobu sett. of Absheron dist., AZ0100 Baku, Azerbaijan. [3]Azerbaijan University of Architecture and Construction, Ayna Sultanova St.5, Baku AZ1073, Azerbaijan. [4]Khazar University, 41 Mahsati Str., Baku AZ1096, Azerbaijan. [5]Jožef Stefan institute, Jamova cesta 39, 1000 Ljubljana, Slovenia. [6]Faculty of Electrical Engineering - University of West Bohemia in Pilsen, Univerzitní 26, Pilsen 306 14, Czech Republic. [7]Institute of Experimental and Applied Physics- Czech Technical University in Prague, Husova 240/5, Prague 110 00, Czech Republic. [8]Faculty of Mathematics and Physics, University of Ljubljana, Jadranska Cesta 19, 1000 Ljubljana, Slovenia. [9]V. Lashkaryov Institute of Semiconductor Physics NAS of Ukraine, 45 Nauky Ave., Kyiv 03028, Ukraine. [10]V. I. Vernadsky Institute of General and Inorganic Chemistry NAS of Ukraine, Academician Palladin Ave.32/34, Kyiv 03142, Ukraine. ✉email: farid081211@gmail.com; yuyu@isp.kiev.ua

current comparisonsfor initial and irradiated SiPMs. Ref[27]. compared a deep-buried pixel MAPD (15 000 pixels/mm², 8 μm pitch) and a surface-pixel MPPC-S14160-1310PS (10 000 pixels/mm², 10 μm pitch), reporting dark current increases of 740 and 66 000 times, respectively, at 6×10^{12} n_{eq}/cm^2, with photo-signal amplitude ratios of 0.1 and 0.075 and breakdown voltage shifts below 0.5 V. These findings highlight the superior radiation tolerance of deep-buried pixel structures.

Nevertheless, the radiation hardness of deep-buried pixel SiPMs remains insufficiently characterized, with limited studies addressing gamma rays, neutrons, and protons across various pixel pitches[21–24]. Refs[21,22]. examined MAPD-3NK (10 μm pitch, 7 μm pixels) and MAPD-3NM-II (15 μm pitch, 12 μm pixels) under ^{60}Co gamma rays (up to 100 kGy). After irradiation, the dark current of the photodiodes increased by a factor of 13, the breakdown voltage shifted by 80 mV, the capacitance of the photodiodes remained unchanged, and the amplitude of the signal decreased by 13.5%[21]. Ref[21–23]. tested deep-pixel SiPMs (8 μm pitch) with 39 MeV neutrons at $3.9\times10^{12}n_{eq}/cm^2$, observing a 1000-fold dark current rise, yet operational stability persisted. These results underscore the enhanced radiation tolerance of deep-buried pixel designs, necessitating further investigation.

In this work, the radiation resistance of MAPD-3NK2 type SiPMs under neutron irradiation was investigated by analyzing key performance parameters, including dark current, breakdown voltage, capacitance, photosignal amplitude, and amplitude resolution.By systematically evaluating these parameters before and after neutron exposure at different fluences (3.6×10^9, 3.6×10^{10}, 3.6×10^{11}, 3.6×10^{12} n_{eq} /cm²), we aimed to quantify the impact of radiation damage and explore potential mitigation strategies to enhance the long-term reliability of SiPMs in high-radiation environments.

Experimental setup and results

MAPD-3NK2 type SiPMs with deep-buriedpixels structure were used in this experiment. MAPD-3NK2 was produced by Zecotek Photonics Inc. Figure 1 shows the schematic design and equivalent circuit of the device. Itconsisted of several silicon layers, beginning with an n-type silicon substrate, followed by: a heavily doped n^+-type layer on the substrate, a lightly doped n-type epitaxial layer with a thickness of 7 μm, n^+-type pixels doped with donor type impurities, an n^--type region lightly doped with donor type impurities, a p-type epitaxial layer with a thickness of 4 μm, a heavily doped p^+-type layer, and a dielectric layer.

When a negative potential is applied to a heavily doped p^+-type layer relative to the substrate, ahigh field region is formedat the boundary of the p-type epitaxial layer and n^+-type pixels, enabling avalanche multiplication of charge carriers.

The concentration of impurities in the n^--type layer is chosen so that non-depleted individual channels are formed under the pixels, providingsufficientresistance to quench the avalanche process. Each pixel has a diameter of 7 μm and a spacingof 3 μm, resulting in a sensitive area of 3.7×3.7 mm² with a pixel density of 10 000 pixels/mm² (totaling 1.33×10^5 pixels). The photon detection efficiency (PDE) of the MAPD-3NK2 is approximately 23% (for 420 nm) at 1 V overvoltage[9].

The dark current and capacitance of SiPM were performed usingaKeithley 6487 SourceMeter andanImmitance meter E7-20 device, as shown in Fig. 2. Position 1 was used for measurement current –voltage (I-V) characteristics & amplitude distribution, whilePosition 2 was used for capacitance – voltage (C-V) characteristics.

Optical performance of SiPMs were investigated with LED (420 nm wavelength) diode, CAEN-5720 ADC, Tektronix 3101 signal generator, Ortec FTA 820 amplifier and Keithley 6487.Rectangular pulses of 30 ns duration, 5 kHz frequency, and 4.5 V amplitude were used.The number of photoelectrons per pulse was calculated with MPPC-S13360-3025CS (25 μmpixel pitch, PDE ~ 25% at 450 nm, 3×3 mm²active area), yielding 1100 photoelectrons per pulse for testing the SiPMs[28].

The capacitance measurements were performed using an Immitance meter E7-20 device. A 1 MHz signal with an amplitude of 40 mV was supplied from the Impedance E7-20 device. The measurement error of the Impedance E7-20 device was 1.5 pF. A Keithley 6487 was used as an external voltage source to apply a wide range of bias voltages to the photodiodes.

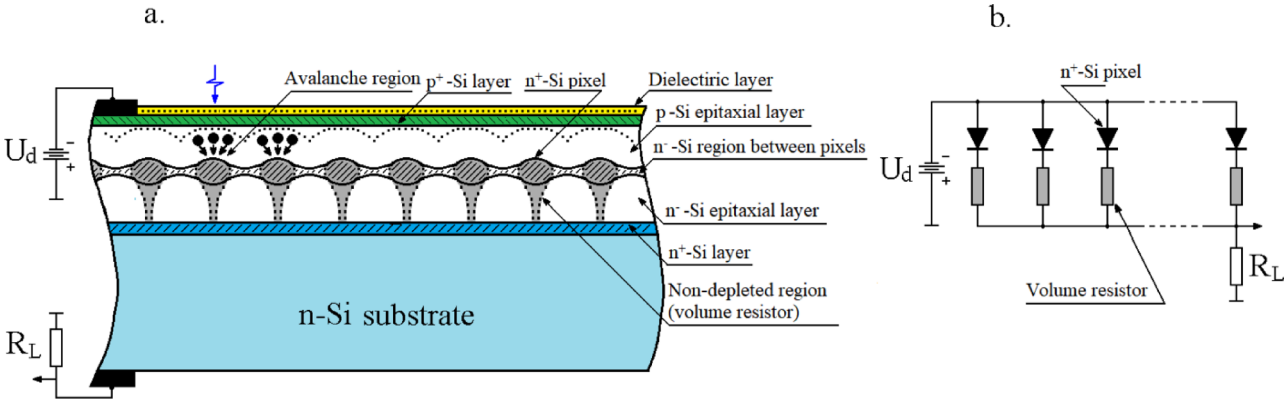

Fig. 1. A schematic design (**a**) and equivalent circuit (**b**) of the MAPD-3NK2.

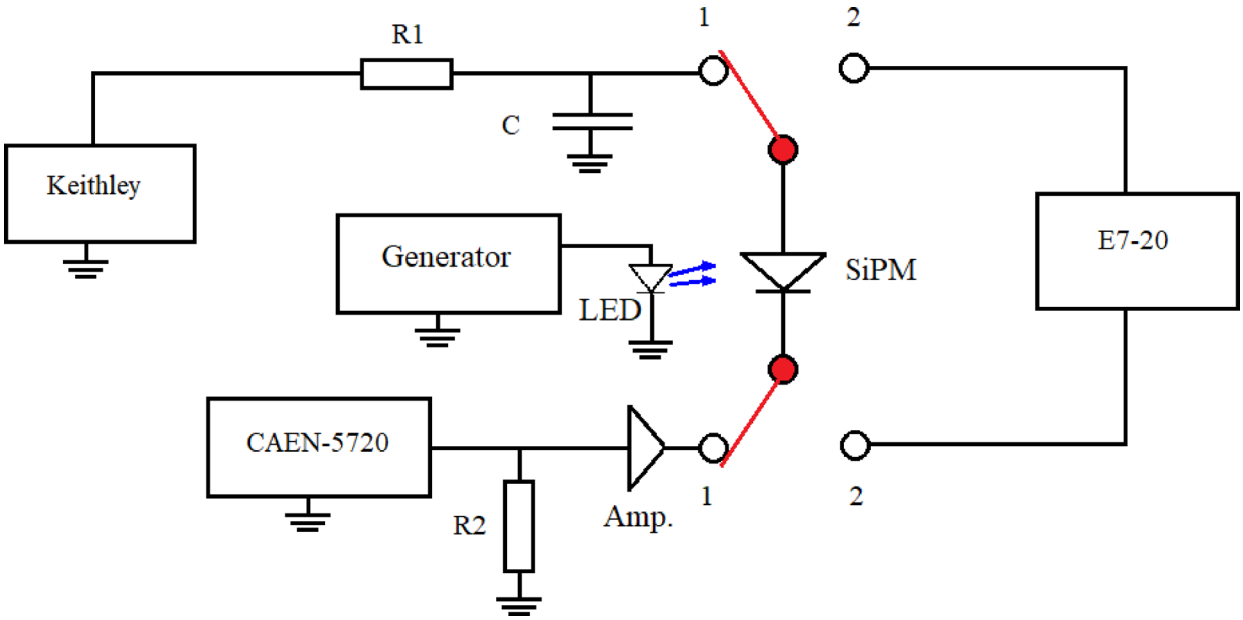

Fig. 2. Experimental setup for current – voltage characteristics, amplitude distribution (1), and capacitance – voltage characteristics (2).

Fig. 3. Photo of MAPD-3NK2 photodiodes.

MAPD-3NK2 photodiodes were irradiate with neutronsat the Jožef Stefan Institute (JSI) TRIGA reactor in the Triangular Irradiation Channel 2 (TIC 2)[29]. Target fluences were 1×10^{10}, 1×10^{11}, 1×10^{12} and 1×10^{13} n/cm^2, achieved at the reactor power levels of 1 W, 10 W, 100 W and 1 kW for 253 s, to reduce the uncertainties related with the sample insertion and withdrawal time of about 1s. As the JSI TRIGA is a thermal reactor, the real neutron fluence is significantly smaller than the fluence of the 1 MeV neutron equivalent damage in silicon[30]. To account for this, a detailed Monte Carlo particle transport simulation of the irradiation experiment was performed using the MCNP code[31], together with the ENDF/B-VIII.0 nuclear data libraries[32]. Normalization was based on reactor log data (control rod positions and power levels), following the methodology[33]. Eachirradiation included two SiPM samples (shown in Fig. 3) enclosed in a polyethylene container for repeatability and redundancy.

The calculations also allowed us to determine the potential variability of the neutron flux within the channel, since no control of the exact sample position was possible, and the TIC 2 being larger than the polyethylene container. Figure 4 shows the simulated total neutron flux (left) and 1 MeV equivalent neutron flux (right) based on the ASTM E722 standard for irradiation at reactor power of 1 W.

A total eight photodiodes were irradiated. After irradiation, samples were stored in a container for two days to allowfor decay of activation products, after which their diode characteristics were measured. The surface dose rate, measured with an Automess 6150 AD, was 3 μSv/hour, dominatedby gamma rays from gold (Au) used in the SiPM housing and pins. Measurements were then carried out at (23 ± 0.5) °C at intervals of 2, 6, 12, 19, 37, 73, 100, and 130 days to track recovery dynamics.

Figure 5 shows the dependence of the capacitance of MAPD-3NK2 photodiodes on the applied voltage. As the applied voltage increases, a space-charge region begins to form between the p-type epitaxial layer, the n-type pixels, and the n-type epitaxial layer. Due to the high dopant concentration in the n-type pixels, theyremain undepleted, and the space-charge region extended primarily within the p-type epitaxial layer. At 20 V, the p-type epitaxial layer was largely depleted, reducing capacitance as the space-charge region widens. When the applied voltage reached 57 V, the depletion region began to extend into the first n-type epitaxial layer, particularly in the regions between the pixels. As the applied voltage increased further, it primarily contributed to the depletion of

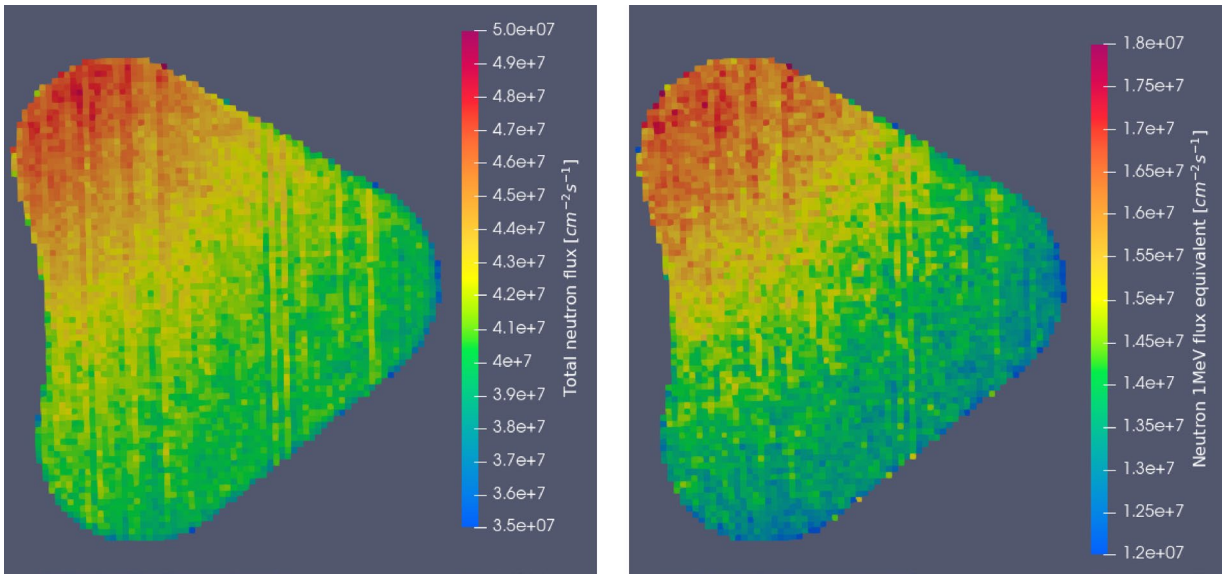

Fig. 4. Total neutron flux (left) and neutron 1 MeV equivalent flux (right) in the TIC 2 during irradiation at 1 W.

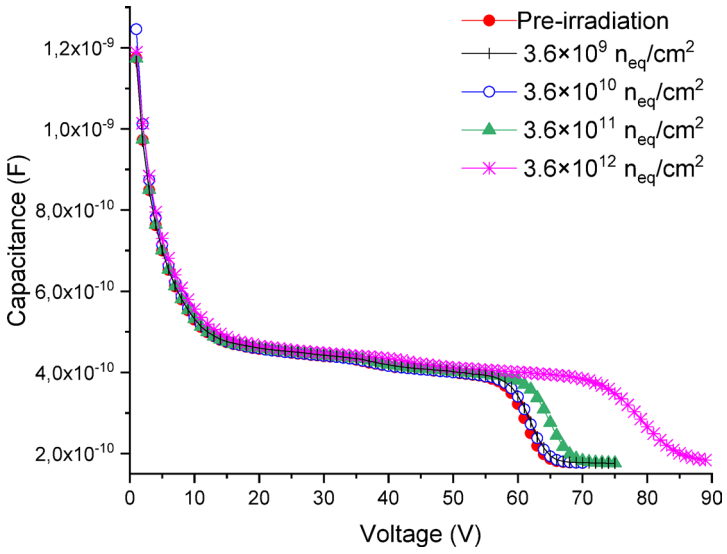

Fig. 5. Capacitance-voltage characteristics of MAPD-3NK2 photodiodes irradiated at various fluences.

the n-type epitaxial layer, while the space-charge region did not extend significantly into the pixels themselves due to their high doping concentration. By 68 V, it reached the lower portions of the n-type pixels, and at 70 V, both the n-type and p-type epitaxial layers were fully depleted, covering the photodiode's active region. Beyond this voltage, further increased in the applied voltage did not affect the depletion process, and the photodiode capacitance stabilized at (176 ± 1.5) pF.

No significant capacitance changes were observed at fluences of $3.6\times10^{9}$and $3.6\times10^{10}$$n_{eq}/cm^2$. Significant changes in capacitance were observed following neutron irradiation at a fluence of $3.6\times10^{11}$$n_{eq}/cm^2$, particularly in the 62–68 V voltage range. The voltage at which the space-charge region fully encompassed both epitaxial layers was 71 V at a fluence of $3.6\times10^{11}$$n_{eq}/cm^2$, respectively. The corresponding capacitance of the irradiated MAPD-3NK2 was at (176 ± 1.5) pF. The change in capacitance within the specified voltage range of (72–88) V was attributed to processes occurring in the first n-type epitaxial layer and n^- type region between pixels at a fluence of 3.6×10^{12} n_{eq}/cm^2, respectively. Even at an applied voltage of 89 V following a fluence of 3.6×10^{12} n_{eq}/cm^2, the capacitance of the photodiode did not reach full saturation. It should be noted that at this voltage, the breakdown process in the diode began, resulting in a high internal gain. However, applying a voltage higher than this threshold led to an uncontrolled breakdown event. Therefore, it was not possible to apply a voltage above 89 V to the MAPD-type photodiode, which was required to achieve full saturation. It is likely related to

the presence of radiation-induced defects that exhibit n-type behavior within the n^--type epitaxial layer and n^- type region between pixels. As a result, the depletion voltage of the n^--type epitaxial layer increased. The corresponding capacitance of the irradiated MAPD-3NK2 was (183 ± 1.8) pF at 89 V. Even in this case, the change in the capacitance of the MAPD-3NK2 photodiode was reduced by 4%. This change was within the acceptable measurement error range.

Figure 6 shows the I-V characteristics of the MAPD-3NK2 photodiode as a function of neutron fluences. MAPD-3NK2 type photodiode was fully depleted at 70 V (for non-irradiated and3.6×10^9-3.6×10^{10} n_{eq}/cm^2) andincreasing the applied voltage up to 84 V did not significantly increase the dark current of the SiPM. The generation of dark current was influenced by thermal carriers, radiation defects, and contamination. As the applied voltage approached of equaled the breakdown voltage, carriers were accelerated by an electric field between p-type epitaxial layer and pixels. This accelerated charge produces electrons and holes via impact ionization. Due to this process, the dark current of the SiPM increased dramatically.

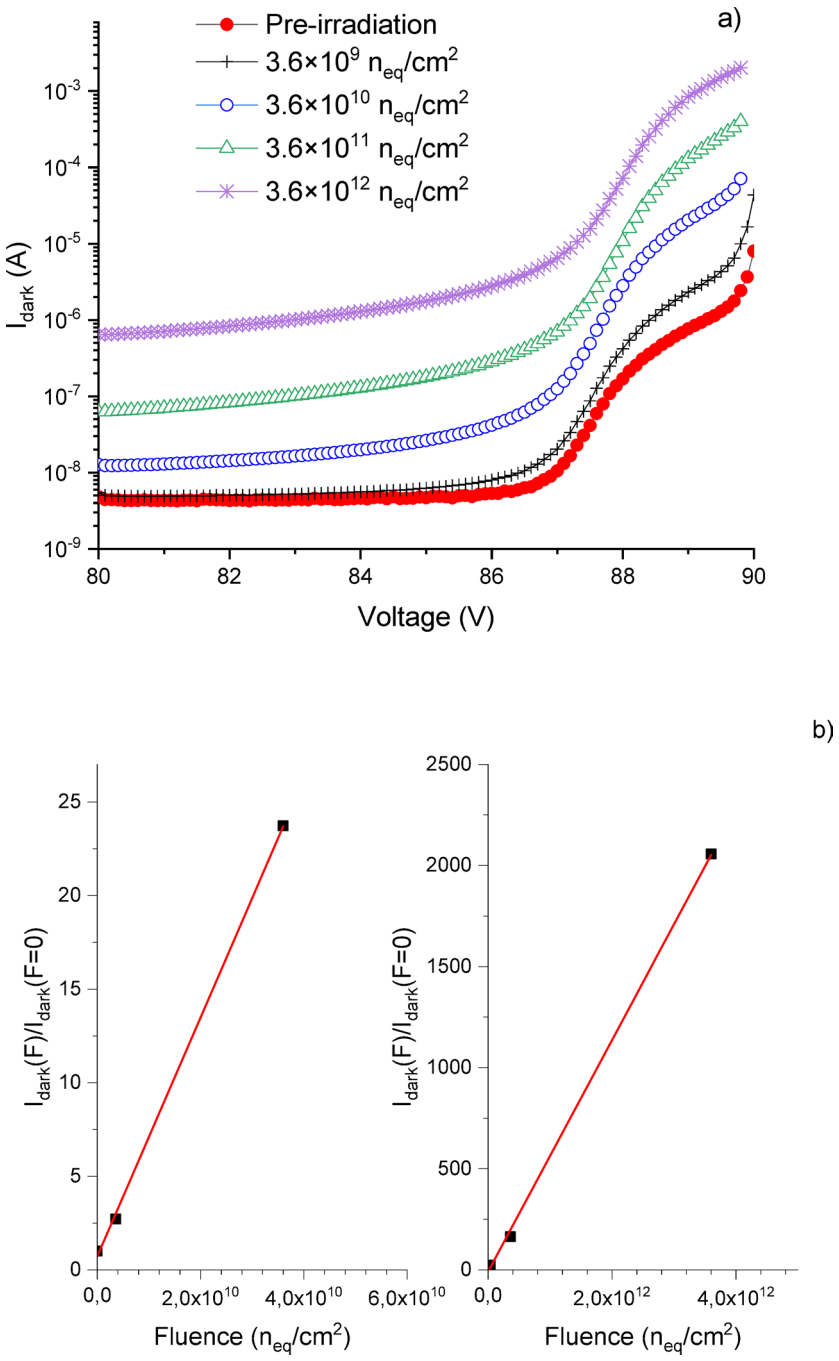

Fig. 6. (**a**) Current-voltage characteristics of the MAPD-3NK2 photodiode irradiated at various neutron fluences; (**b**) dependence of the dark current ratio at 1 V overvoltage on neutron fluence.

The avalanche process was quenched by the bulk resistance of the n-type epitaxial layer under each pixel. At the same time, since the pixels were not depleted, charges accumulated in the potential wells formed beneath them, contributing to the quenching of the avalanche process. This dual quenching mechanism allowed the pixel of MAPD-3NK2 photodiode to operate in the overvoltage mode (88–89 V), where the rate of dark current increasediminished due to effective avalanche suppression.

Neutron irradiation increased the dark current of MAPD-3NK2 photodiodes proportionally to the fluence, primarily due to deep-level traps introduced by radiation damage. These defects enhanced carrier generation in the depletion region, elevating leakage current across all voltage ranges.

Dark current comparisons for neutron-irradiated MAPD-3NK2 photodiodes were conducted at 1 V overvoltage. The dark current increased by factors of 2.7 to 2 060 across the fluence range of $3.6\times10^{9}$to 3.6×10^{12} n_{eq}/cm^2. Figure 6b(right) shows the dark current ratio for fluences from 0 to $3.6\times10^{12}n_{eq}/cm^2$, while Fig. 6b(left) details the ratio for lower fluences (0 to $3.6\times10^{10}n_{eq}/cm^2$).

The dark current exhibited a linear dependence on irradiation fluence, described by the equation: $I_{dark}(nA) = (-8.66\pm11.45) + (5.72\times10^{-10}\pm7.07\times10^{-12})\times F$, where (F) is the fluence (n_{eq}/cm^2) and I_{dark} is the dark current (nA).

Breakdown voltage was extracted from the maximum of the differential ratio dI/(dU×I) (Fig. 7). The pre-irradiation breakdown voltage was 87.50 V. No measurable shift occurred up to 3.6×10^{11} n_{eq}/cm^2; at 3.6×10^{12} n_{eq}/cm^2, the breakdown voltage increased by (0.37 ± 0.08) V. This shift is attributed to increased voltage drop across the quenching resistance and possible junction heating from elevated dark current[34].

The avalanche process was suppressed by a quenching resistor, leading to a decrease in dI/(dU×I) and a minimum value at the optimum voltage, where dark current changes were minimized. Beyond this point, higher voltagescaused an uncontrolled avalanche, increasing the ratio. No significant breakdown voltage shift was observed for neutron fluences from 3.6×10^{9} n_{eq}/cm^2 to 3.6×10^{11} n_{eq}/cm^2. The pre-irradiation, the breakdown voltage of the MAPD-3NK2 photodiode was 87.5 V, and after neutron irradiation with a fluence of $3.6\times10^{12}n_{eq}/cm^2$, the breakdown voltage of the photodiode increased by (0.37 ± 0.08) V, to 87.87 V.

The breakdown voltage in semiconductors depends on factors such as doping concentration, temperature, space-charge region width, and pixel diameter[34]. Capacitance measurements of irradiated MAPD-3NK2 photodiodes indicated significant changes in carrier concentration within the p-type and n-type epitaxiallayer. The increased dark current following neutron irradiation caused substantial voltage drops across the quenching resistance, reducing the effective bias voltage across the pixels.

Consequently, higher external voltages must be applied to achieve breakdown conditions, resulting in an apparent increase in measured breakdown voltage. Furthermore, the increase in dark current can heat the p–n junction, which in turn contributes to a rise in breakdown voltage[34].

The impact of neutron irradiation on the photosignal amplitude of MAPD-3NK2 photodiodes was investigated using a 420 nm light-emitting diode (LED) with a 3 × 3 mm^2 light spot. The LED was driven with pulses of 30 ns duration, 3 kHz frequency, and 4.5 V amplitude. The photosignal was amplified using an Ortec FTA 820 amplifier and digitized with a CAEN-5720 analog-to-digital converter (ADC) set to a 100 ns integration window. During the measurements, an MPPC-S13360-3025CS photodiode was used to determine the number of photoelectrons generated per pulse, with approximately 1100 photoelectrons corresponding to each pulse. MPPC-S13360-3025CS photodiode was used as reference photodiode for all the amplitude distribution measurements. During the measurement of the amplitude distribution of the MAPD-3NK2 photodiodes,

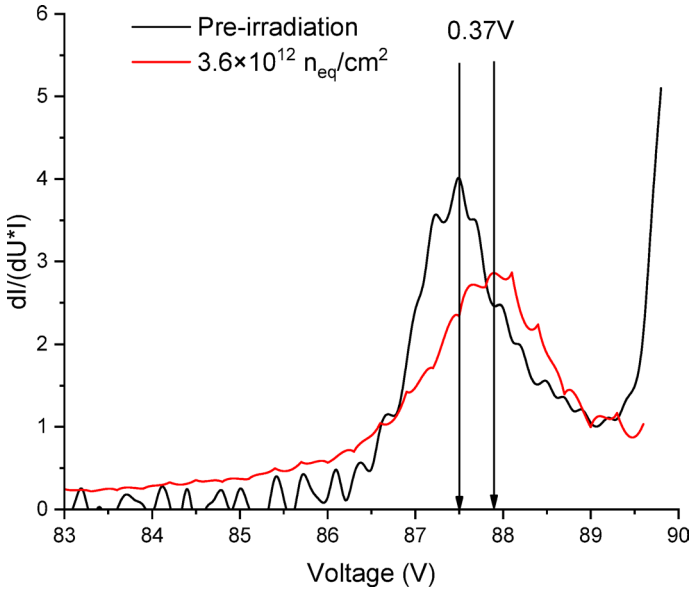

Fig. 7. Voltage dependence of the differential ratio dI/(dU×I) dI/(dU×I)dI/(dU \times I)for the MAPD-3NK2 photodiode before and after neutron irradiation at a fluence of $3.6\times10^{12}n_{eq}/cm^2$.

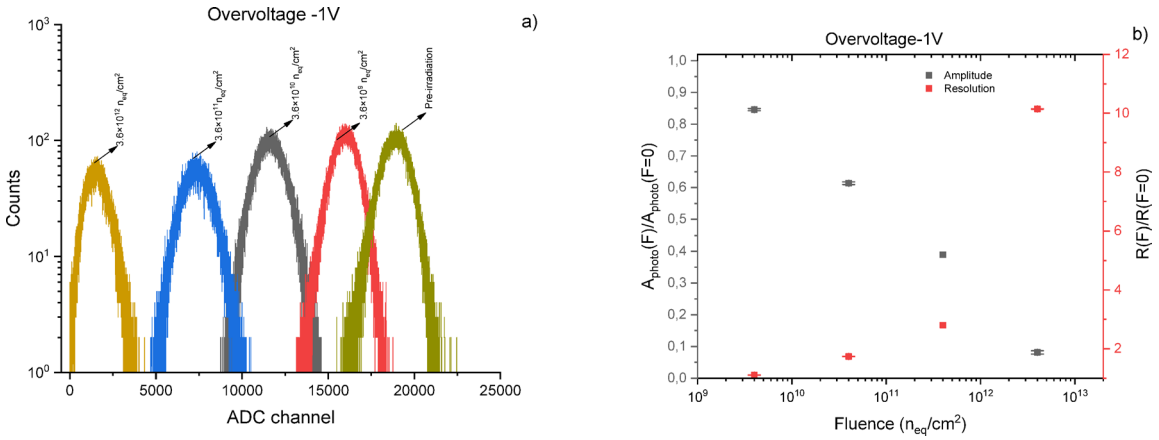

Fig. 8. (**a**) Photosignal amplitude distribution at 1 V overvoltage for both irradiated and pre-irradiation MAPD-3NK2 photodiodes; (**b**) dependence of the photosignal amplitude and FWHM ratio of MAPD-3NK2 photodiodes on neutron fluence.

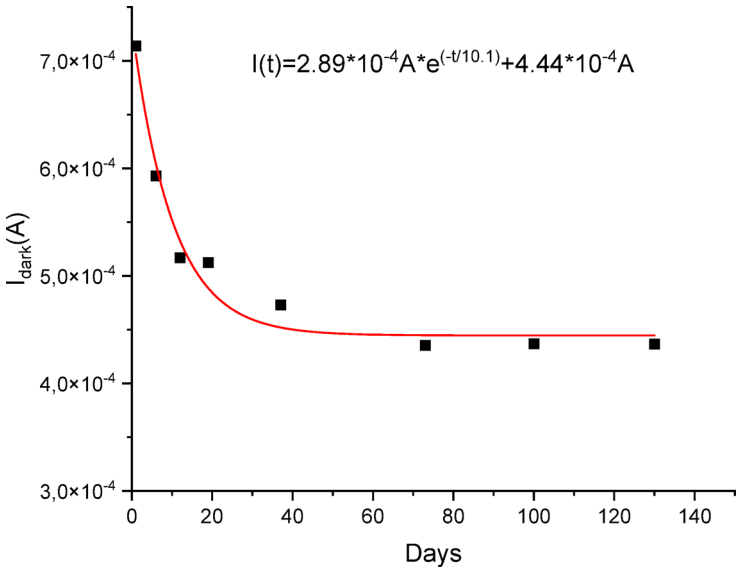

Fig. 9. Temporal variation of dark current in an MAPD-3NK2 photodiode irradiated with neutrons at a fluence of $3.6\times10^{12}n_{eq}/cm^2$ under an overvoltage of 1 V.

an overvoltage of 1 V was applied to the device. Due to the high dark current at high radiation fluence of ($3.6\times10^{11}n_{eq}/cm^2$ and $3.6\times10^{12}n_{eq}/cm^2$), a short the measurement duration was chosen in order to minimize the induced temperature effects.

Using a 420 nm LED, the photosignal amplitude was measured at 1 V overvoltage (Fig. 8a). The amplitude decreased from 18,953 ADC channels (unirradiated) to 1,864 channels at 3.6×10^{12} n_{eq}/cm^2. As shown in Fig. 8b, the signal amplitude decreased by (90.1 ± 0.4)%, while the FWHM ratio increased tenfold. The degradation is attributed to carrier trapping/recombination at radiation-induced defects and pixel occupation by excess dark carriers[21,24,35].

The observed reduction in photosignal amplitude and resolution was primarily due to radiation-induced defects from neutron interactions, which act as charge carrier traps and recombination centers, diminishing the number of carriers contributing to the signal[21,24,35]. Additionally, pixel occupation by charge carriers from these defects or incomplete avalanche quenching may prevent photoelectron detection, further reducing the photosignal amplitude.

The time-dependent behavior of dark current and capacitance-voltage (C-V) characteristics was examined for a MAPD-3NK2 photodiode irradiated at $3.6\times10^{12}n_{eq}/cm^2$ and maintained at 23 °C. The dark current at 1 V overvoltage was monitored over time, as shown in Fig. 9.

The dark current decreased over time, with a 34% reduction after 30 days, corresponding to an average daily decrease of 6.51 µA. From 30 to 70 days post-irradiation, an additional 5% reduction occurred, at a rate of 1.04

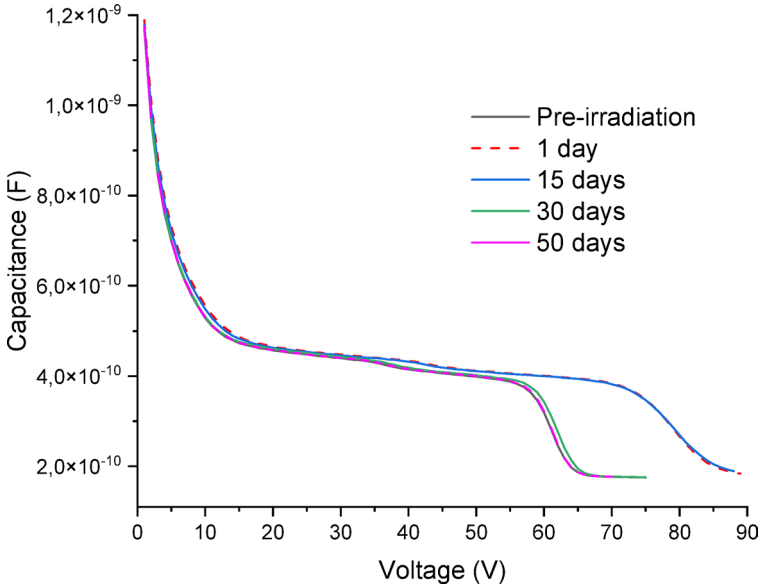

Fig. 10. Capacitance-voltage characteristics of a MAPD-3NK2 photodiode irradiated at a neutron fluence of $3.6 \times 10^{12} n_{eq}/cm^2$, measured at various time intervals post-irradiation.

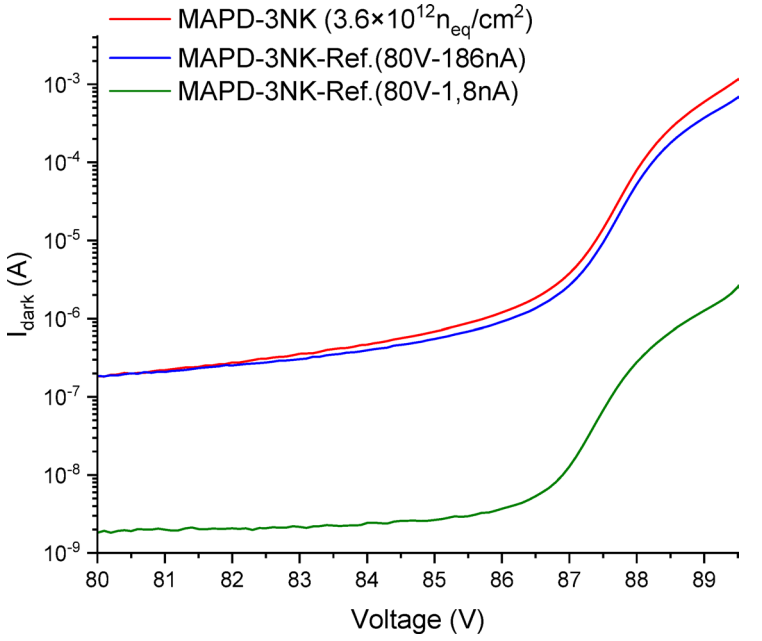

Fig. 11. Current-voltage characteristics of MAPD-3NK2 photodiodes: irradiated at a neutron fluence of 3.6×10^{12} n_{eq}/cm^2, unirradiated with natural dark current, and unirradiated with artificially increased dark current using a 720 nm LED light source.

μA/day. This recovery was attributed to partial annealing of radiation-induced defects at room temperature. The dark current followed an exponential decay, described by.

$I(t) = 2.89 \times 10^{-4} A \times e^{(-t/10.1)} + 4.44 \times 10^{-4} A$, with a time constant of 10.1 days.

From 70 to 130 days post-irradiation, the dark current remained stable within measurement uncertainty, indicating that radiation-induced defects reached a metastable equilibrium, marking the completion of observable room-temperature annealing processes.

Figure 10 illustrates the capacitance-voltage dependence of the neutron-irradiated photodiode at various time intervals post-irradiation. Thirty days after irradiation at $3.6 \times 10^{12} n_{eq}/cm^2$, the capacitance matched that of an unirradiated photodiode, likely due to the annealing of some radiation-induced defects[19].

To investigate the mechanisms of radiation-induced defects on MAPD-3NK2 photodiode performance, an unirradiated photodiode was tested with its dark current artificially increased for comparison with irradiated samples.

Figure 11 illustrates the current-voltage (I-V) characteristics of MAPD-3NK2 photodiodes, comparing an unirradiated photodiode, one with artificially increased dark current, and one irradiated at $3.6\times10^{12}n_{eq}/cm^2$. The dark current of the unirradiated photodiode was 1.8 nA at 80 V prior to artificial enhancement.The dark current of the unirradiated photodiode was elevated to 186 nA at 80 V using a 720 nm LED light source powered by a constant voltage source. This wavelength was selected to generate charge carriers uniformly throughout the photodiode's active volume, mimicking the carrier distribution induced by neutron irradiation defects. The chosen current matched the stabilized dark current of the irradiated photodiode at 80 V. The I-V characteristics of the irradiated and artificially modified photodiodes exhibit similar trends, indicating comparable effects on performance.

Figure 12 presents the voltage dependence of the differential ratio dI/(dU×I) dI/(dU×I)dI/(dU \times I) for an unirradiated MAPD-3NK2 photodiode in its initial state and with artificially increased dark current using a 720 nm LED. The breakdown voltage, initially 87.42 V, increased to 87.78 V under illumination, a shift of (0.36 ± 0.07) V. This shift aligned with the (0.37 ± 0.08) V increase observedin photodiodes irradiated at $3.6\times10^{12}n_{eq}/cm^2$. These results indicated that an increase in dark current led to a higher breakdown voltage, likely due to a voltage drop across the space-charge region resistance within the photodiode and substantial heating of the p–n junction caused by the dark current.

Figure 13 illustrates the photocurrent-voltage characteristics of MAPD-3NK2 photodiodes, comparing samples irradiated at $3.6\times10^{12}n_{eq}/cm^2$ with unirradiated samples, both with and without artificially increased dark current. Photocurrent was generated using a 420 nm LED light source driven by a Tektronix AFG 3101 C signal.

generator, producing pulses with a 100 ns duration, 10 kHz frequency, and 6 V amplitude. The photocurrent flowing from the neutron-irradiated MAPD-3NK2.

photodiode at a voltage of 80 V was 22.5 nA while the photocurrent flowing from the artificially increased MAPD-3NK2 photodiode was 31 nA.

The photocurrent-voltage characteristics of the photodiodes were similar up to the breakdown voltage. However, at 1 V overvoltage, the irradiated photodiode exhibited an approximately 18% reduction in photocurrent compared to the unirradiated sample with artificially increased dark current. This decrease was attributed to trapping and recombination centers formed by radiation-induced defects[21,24,30,31].

The primary decrease in photocurrent was attributed to a sharp increase in the dark current of the MAPD photodiode. The excess charge carriers contributing to this increased dark current may occupy the pixels (or result from incomplete quenching of the avalanche process), thereby preventing the detection of photoelectrons and leading to a reduction in photocurrent[21,24,35].

Conclusion

Neutron irradiation tests on MAPD-3NK2 photodiodes with deep-buried pixel structures, conducted at fluences ranging from $3.6\times10^{9}$to $3.6\times10^{12}n_{eq}/cm^2$, demonstrated robust performance under challenging radiation conditions. The study observed a dark current increase by factors of up to 2 060, a modest breakdown voltage shift of (0.37 ± 0.08) V, a photosignal amplitude reduction of (90.1 ± 0.4)%, and a tenfold increase in amplitude resolution. Encouragingly, post-irradiation annealing at room temperature for 40 days reduced the dark current by approximately 35% for samples exposed to $3.6\times10^{12}n_{eq}/cm^2$, highlighting the potential for partial recovery. Comparative tests with an unirradiated photodiode, where dark current was artificially elevated, mirrored

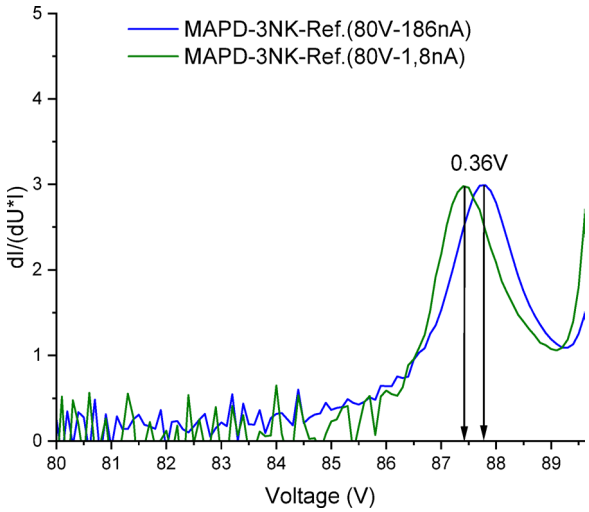

Fig. 12. Voltage dependence of the differential ratio dI/(dU×I) for the MAPD-3NK2 photodiode, comparing natural dark current with artificially increased dark current induced by a 720 nm LED light source.

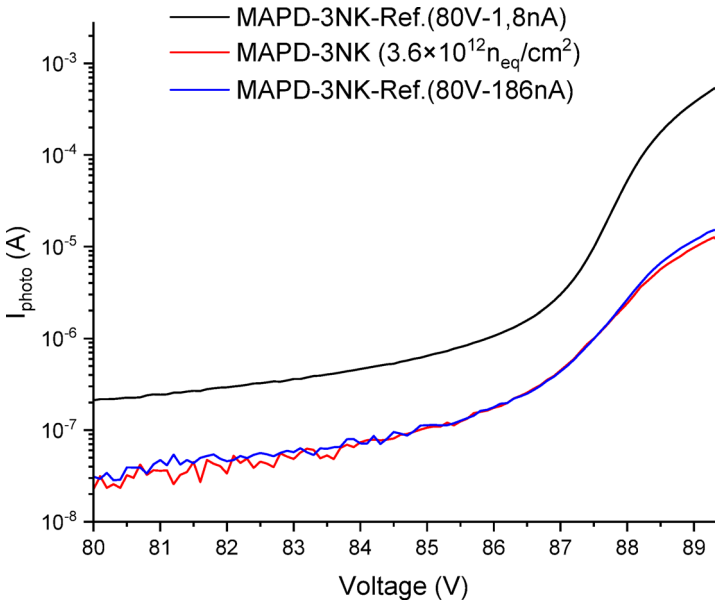

Fig. 13. Photocurrent-voltage characteristics of MAPD-3NK2 photodiodes: irradiated at a fluence of 3.6×10^{12} $n_{eq}/cm^2$and unirradiated, with and without artificially increased dark current using a 720 nm LED light source.

the changes observed in irradiated samples, confirming that increased dark current is the primary driver of performance degradation. This effect is likely due to excess charge carriers occupying pixels or incomplete avalanche quenching, which impedes photoelectron detection.

The MAPD-3NK2 photodiodes, with an 11 µm thick epitaxial layer, exhibited significantly better radiation hardness compared to surface-pixel SiPMs of equivalent pixel density[26,27]. The depletion region of MAPD-3NK2 photodiode was approximately five times thicker than that of surface-pixel SiPMs[26]. However, the results obtained for the MAPD-3NK2 photodiodes showed that the increase in dark current was at least five times lower compared to surface-pixel SiPMs with the same pixel density[26,27]. In addition, the shift in breakdown voltage for the MAPD-3NK2 devices was smaller than that observed in surface-pixel SiPMs[26,27]. Obtained results indicated that MAPD-3NK2 photodiodes with deep pixels exhibit greater radiation hardness than surface-pixel SiPMs at a fluence of 3.6×10^{12} n_{eq}/cm^2.MAPD-3NK2 photodiodes can therefore be effectively used in experiments where SiPMs with surface-pixel were currently applied e.g. Ring Imaging Cherenkov detectors, the Belle II experiment, NA61@CERN, CBM@FAIR, BM@N and NICA heavy-ion collision experiments[23–27].

Future improvements, including reducing the epitaxial layer thickness to 7 µm, are expected to further minimize dark current and breakdown voltage variations under high fluences[34], expanding the applicability of these photodiodes to even more extreme radiation environments and offer a reliable and efficient solution for advanced detector systems. The results of this study highlight the potential of MAPD-3NK2 photodiodes to advance high-energy physics and related fields, paving the way for their integration into next-generation radiation-hard detection technologies.

Data availability

All data generated or analysed during this study are included in this published article.

Received: 21 May 2025; Accepted: 15 October 2025
Published online: 20 November 2025

References

1. Lecoq, R. Recent developments in PET imaging technology. *IEEE Trans. Nucl. Sci.* **67** (6), 1234–1245 (2020).
2. Simon, F. Silicon photomultipliers in particle and nuclear physics. *Nuclear Instruments Methods Phys. Res. Sect. A Accelerat. Spectromet. Det. Assoc. Equip.* **926**, 85–100. https://doi.org/10.1016/j.nima.2018.11.042 (2019).
3. Jones, A. H. et al. Radiation tolerance of SiPMs in space applications. *Space Sci. Rev.* **216** (3), 55–67 (2021).
4. CollazuolG. SiPMs: Performance, applications, and challenges. *Nuclear Instruments Methods Phys. Res. A*. **926**, 16–35 (2019).
5. Ahmadov, F. et al. Performance of LaBr3(Ce) scintillator with MAPD readout in the gamma-ray energy range of 0.1–7.0 MeV. *Radiat. Detect. Technol. Methods*. https://doi.org/10.1007/s41605-025-00547-3 (2025).
6. Holik, M. et al. Study of dynamic time over threshold (DTOT) method for application in spectroscopy signal analysis toward a low-complexity front-end electronics with high spectroscopy resolution and wide energy range. *IEEE Trans. Nucl. Sci.* **72** (3), 749–756. https://doi.org/10.1109/TNS.2024.3477748 (2025).
7. A.Sadigov, F. et al. Performance of styrene polymerized plastic scintillator with micropixel avalanche photodiode. *Radiat. Measure.* **171**, 107061. https://doi.org/10.1016/j.radmeas.2024.107061 (2024).
8. Holik, M. et al. Gamma ray detection performance of newly developed MAPD-3NM-II photosensor with LaBr3(Ce) crystal. *Sci. Rep.* **12**, 15855. https://doi.org/10.1038/s41598-022-20006-z (2022).

9. Nuruyev, S. et al. Performance of silicon photomultipliers at low temperature. *J. Instrum.* **15** (03), C03003. https://doi.org/10.1088/1748-0221/15/03/C03003 (2020).
10. Ahmadov, F. et al. Investigation of parameters of new MAPD-3NM silicon photomultipliers. *JINST* **17** (C01001). https://doi.org/10.1088/1748-0221/17/01/C01001 (2022).
11. Sadigov, A. Z. et al. Improvement of parameters of micro-pixel avalanche photodiodes. *JINST* **17** P07021. (2022).
12. Holik, M. et al. Investigation of the possibility of a new detector based on SiPM in nuclear forensics. *J. Instrum.* **18** (1), C01015. https://doi.org/10.1088/1748-0221/18/01/c01015 (2023).
13. Nuruyev, S. et al. Neutron/gamma scintillation detector for status monitoring of accelerator-driven neutron source IREN. *Nuclear Eng. Technol.* https://doi.org/10.1016/j.net.2023.12.020
14. Moll, M. Radiation damage in silicon particle detectors. *Nuclear Instruments Methods Phys. Res. B*. **186**, 100–110 (2002).
15. Yamamoto, K. et al. Neutron irradiation effects on silicon photomultipliers. *IEEE Trans. Nucl. Sci.* **64** (8), 2078–2085 (2017).
16. Parker, S. I. et al. Radiation effects in semiconductor detectors. *Annu. Rev. Nucl. Part. Sci.* **58**, 447–468 (2008).
17. Merzi, S. et al. Radiation damage on silicon photomultipliers from ionizing and Non-Ionizing radiation of Low-Earth orbit operations. *Sensors* **24** (15), 4990. https://doi.org/10.3390/s24154990 (2024).
18. Zhang, Y. et al. Radiation characterization of SiPMs for HERD PSD. *Nuclear Instruments Methods Phys. Res. A* **1070** (1), 170035. https://doi.org/10.1016/j.nima.2024.170035 (2025).
19. Consuegra Rodríguez, D. et al. Characterization of neutron-irradiated SiPMs down to liquid nitrogen temperature. *Eur. Phys. J. C.* **84**, 970. https://doi.org/10.1140/epjc/s10052-024-13302-7 (2024).
20. Merzi, S. et al. Radiation damage on silicon photomultipliers from ionizing and Non-Ionizing radiation of Low-Earth orbit operations. *Sensors* **24**, 4990. https://doi.org/10.3390/s24154990 (2024).
21. Ahmadov, F. et al. Investigation of the gamma radiation resistance of MAPD-3NK and MPPC-S12572-10P SiPMs. *Radiation Measure.* **183**, 107422. https://doi.org/10.1016/j.radmeas.2025.107422 (2025).
22. Ahmadov, F. et al. A gamma-ray spectrometer based on MAPD-3NM-2 and $LaBr_3$(ce) and LSO scintillators for hydrogen detection on planetary surfaces. *Sci. Rep.* **15**, 2823. https://doi.org/10.1038/s41598-025-85845-y (2025).
23. Kushpil, V. et al. *J. Phys. : Conf. Ser.* **675** 012039 (2016).
24. Garutti, E., Gensch, M., Klanner, R., Ramilli, M. & Xu, C. Afterpulse effect in SiPM and neutron irradiation studies. In *2014 IEEE Nuclear Science Symposium and Medical Imaging Conference (NSS/MIC)* 1–7. https://doi.org/10.1109/NSSMIC.2014.7430746 (2014).
25. Ulyanov, A. & Murphy, D. Joseph Mangan. et al. Radiation damage study of SensL J-series silicon photomultipliers using 101.4 MeV protons. *Nuclear Instruments Methods Phys. Res. Sect. A Accelerat. Spectromet. Det. Assoc. Equip.* **976**. https://doi.org/10.1016/j.nima.2020.164203 (2020).
26. Heering, A. et al. Effects of very high radiation on SiPMs. *Nuclear Instruments Methods Phys. Res. Sect. A Accelerat. Spectromet. Det. Assoc. Equip.* **824**.https://doi.org/10.1016/j.nima.2015.11.037 (2016).
27. Mikhaylov, V. et al. *JINST* **15** C02005 (2020).
28. https://www.hamamatsu.com/eu/en/product/optical-sensors/mppc/mppc_mppc-array/S13360-3025CS.html
29. Ambrožič, K., Žerovnik, G. & Snoj, L. Computational analysis of the dose rates at JSI TRIGA reactor irradiation facilities. *Appl. Radiation Isot. Volume*. **130**, 140–152. https://doi.org/10.1016/j.apradiso.2017.09.022 (2017).
30. https://store.astm.org/e0722-19.html
31. Werner, C. J. & Bull, J. S. M. C. N. P. Version 6.2 Release Notes. https://doi.org/10.2172/1419730 (2018).
32. Brown, D. A., Chadwick, M. B. & Capote, R. et.al, ENDF/B-VIII.0: The 8th major release of the nuclear reaction data library with CIELO-project cross sections, new standards and thermal scattering data. *Nuclear Data Sheets* **148** 1–142. https://doi.org/10.1016/j.nds.2018.02.001 (2018).
33. Gašper Žerovnik, M., Podvratnik, L. & Snoj On normalization of fluxes and reaction rates in MCNP criticality calculations. *Ann. Nuclear Energy* **63** 126–128. https://doi.org/10.1016/j.anucene.2013.07.045 (2014).
34. Sze, S. M. & Ng, K. Kwok. *Physics of Semiconductor Devices* (John Wiley & Sons, 2007).
35. Spieler, H. Introduction to Radiation-Resistant semiconductor devices and circuits. *AIP Conf. Proc.* **390**, 23–49. https://doi.org/10.1063/1.52282 (1997).

Acknowledgements

This work has received funding from the European Union's Horizon 2022 Research and Innovation Programme under the Marie Sklodowska-Curie's DETMED project (grant agreement ID 101129879).

Author contributions

F. A.—Study design, data collection, and manuscript preparation. A.M, G. A., A. S., Yu.Yu.B.—Study design and manuscript preparation. Z. S—Supervision and review and editing. A. J-Organization of diode radiation. K. A.—Organization of diode radiation. M. H.—Analysis and data duration. F. M., Yu.S.—Data collection, and manuscript preparation. R. A.,S. N.—Analysis, experimental circuit preparation.O.O.—Manuscript preparation.

Declarations

Competing interests

The authors declare no competing interests.

Additional information

Correspondence and requests for materials should be addressed to F.A. or Y.Y.B.

Reprints and permissions information is available at www.nature.com/reprints.

Publisher's note Springer Nature remains neutral with regard to jurisdictional claims in published maps and institutional affiliations.